[8]D. E. Murnick, in *Hyperfine Interactions*, edited by A. J. Freeman and R. B. Frankel (Academic, New York, 1967), p. 637.

[9]L. Grodzins, in *Hyperfine Structure and Nuclear Radiation*, edited by E. Matthias and D. A. Shirley (North-Holland, Amsterdam, 1968), p. 607.

[10]G. M. Heestand, R. R. Borchers, B. Herskind, L. Grodzins, R. Kalish, and D. E. Murnick, Nucl. Phys. A. **133,** 310 (1969).

[11]J. Lindhard, M. Scharff, and H. E. Schiott, K. Dan. Vidensk. Selsk. Mat.-Fys. Medd. **33** (14), 10 (1963).

[12]B. I. Deutch and G. M. Heestand, in *Angular Correlations in Nuclear Disintegrations*, edited by H. Van Krugten and B. Van Nooijen (Rotterdam U. P., Groningen, The Netherlands, 1970), p. 487.

[13]P. Ryge, Ph.D. thesis (University of Wisconsin, Madison, 1971) (unpublished).

[14]H. Frauenfelder and R. M. Steffen, in *Alpha-, Beta-, and Gamma-Ray Spectroscopy*, edited by K. Siegbahn (North-Holland, Amsterdam, 1968), p. 997.

[15]*Nuclear Data*, edited by K. Way (Academic, New York, 1965), Vol. 1.

[16]C. Günther, G. Strube, U. Wehmann, W. Engels, H. Blumberg, H. Luig, R. M. Lieder, E. Bodenstedt, and H. J. Körner, Z. Phys. **183,** 472 (1965).

[17]The value of $A(^{163}\mathrm{Dy})$ was obtained from the EPR data for Dy^{3+} in Rh [D. Davidov, R. Orbach, C. Rettori, D. Shaltiel, L. J. Tao, and B. Ricks, Phys. Lett. A **37,** 361 (1971)].

[18]L. J. Tao, D. Davidov, R. Orbach, and E. P. Chock, Phys. Rev. B **4,** 5 (1971).

[19]Values of g_n were obtained from the table of nuclear moments prepared by V. S. Shirley which appears in Ref. 2, p. 1255.

[20]A. R. Chuhran, A. Li-Scholz, and R. L. Rasera, in Ref. 2, p. 464.

[21]G. Williams and L. L. Hirst, Phys. Rev. **185,** 407 (1969).

[22]K. R. Lea, M. J. M. Leask, and W. P. Wolf, J. Phys. Chem. Solids **23,** 1381 (1962).

[23]C. R. Burr and R. Orbach, Phys. Rev. Lett. **19,** 1133 (1967).

[24]R. Orbach and H. J. Spencer, Phys. Lett. A **26,** 457 (1968).

[25]T. Moriya, J. Phys. Soc. Jap. **18,** 516 (1963).

[26]T. Izuyama, D-J. Kim, and R. Kubo, J. Phys. Soc. Jap. **18,** 1025 (1963).

PHYSICAL REVIEW B VOLUME 7, NUMBER 11 1 JUNE 1973

Nuclear Magnetic Resonance of ^{11}B at the Three Boron Sites in Rare-Earth Tetraborides

J. H. N. Creyghton,* P. R. Locher, and K. H. J. Buschow
Philips Research Laboratories, Eindhoven, The Netherlands
(Received 13 October 1972)

An experimental study has been made of the ^{11}B Knight shift at the three different crystallographic boron sites in polycrystalline NdB_4. The three central transitions strongly overlap and cannot be analyzed, but it was possible to derive three different Knight shifts [+0.33(3), +0.26(4), and +0.23(3) % at 77 K for the sites $4e$, $8j$, and $4h$, respectively, uncorrected for pseudocontact and demagnetization fields] from the satellites, which are separated from each other by their different quadrupole interactions [$\nu_Q=420(6)$ kHz and $\eta=0$ for site $4e$, $\nu_Q=443(10)$ kHz and $\eta=0.51(2)$ for site $8j$, and $\nu_Q=622(6)$ kHz and $\eta<0.05$ for site $4h$, at both 296 and 77 K]. A detailed account is given of the method of extracting the various shift and quadrupole parameters from the powder satellite spectra. We first analyzed LaB_4, in which the shifts are zero ($\pm 0.02\%$) with respect to $Na_2B_2O_4$ and in which the quadrupole interactions are $\nu_Q=343(4)$ kHz and $\eta=0$ for $4e$, $\nu_Q=412(4)$ kHz and $\eta=0.53(1)$ for $8j$, and $\nu_Q=544(4)$ kHz and $\eta=0.045(20)$ for $4h$ (4–300 K). In NdB_4, relatively large anisotropic contributions to the shifts are found to originate mainly from dipolar fields due to the rare-earth magnetic moments. After correction for pseudocontact shifts, the isotropic hyperfine fields at boron per unit spin S are about -2 kG. Preliminary measurements on GdB_4 and HoB_4 give the same sign for this field. An attempt is made to fit the observed isotropic shifts in NdB_4 within the Ruderman–Kittel–Kasuya–Yosida scheme.

I. INTRODUCTION

It is well known that the localized $4f$ moments in rare-earth intermetallic compounds interact via the conduction electrons. For a description of magnetic properties, the Ruderman–Kittel–Kasuya–Yosida (RKKY) model[1] is often used. One of the consequences of this model is a nonuniform conduction-electron-spin polarization which, in the case of crystallographically inequivalent sites, can lead to a difference in spin polarization at these sites.

In principle, Knight-shift measurements of nuclei of nonmagnetic atoms such as ^{27}Al can give experimental evidence of such a nonuniform conduction-electron-spin polarization. The orthorhombic compounds R_3Al_{11} (R is a rare earth) have been studied[2] for this purpose but they are complicated as they have two R and four Al positions, whereas only two overlapping nuclear-magnetic-resonance (NMR) lines were observed.

In some respects the presently investigated tetragonal RB_4 compounds seemed to be better suited for the purpose. Their structure gives rise

to only one R position and three B positions and thus facilitates a complete analysis of the NMR spectra.

In other respects, however, borides are not very suitable for a test of the RKKY theory as the conduction electrons may have appreciable non-s character. Another disadvantage is the fact that for light nuclei, such as boron, contact hyperfine fields are relatively small, compared with the dipolar fields. We observed, for example, rather large anisotropic contributions to the shifts, which could well be ascribed to dipolar fields, originating from the rare-earth magnetic moments. Furthermore, in the case of an anisotropic susceptibility, this dipolar field makes a small contribution to the isotropic part of the observed shifts, which cannot be distinguished from isotropic contact fields. In the literature on the Knight shift, little or no attention is paid to this effect. It is known as the pseudocontact interaction.[3]

A more serious difficulty, also associated with the weakness of the contact fields, is the impossibility of observing any difference in Knight shift for the three boron sites in the isostructural nonmagnetic compound LaB_4 (using magnetic fields of about 16 kG). This essentially rules out the possibility of answering the question whether, for the RB_4 compounds, a nonuniform-polarization model gives a better description of the experimental results than the more simple model of uniform polarization.[4] This latter model has been used previously to describe Knight shifts as long as there was no constraining reason for using a more complicated model. Hence we shall present the shift data as hyperfine fields per unit spin S, a model-independent quantity.[5]

For the reasons just mentioned, the main emphasis in our paper will not consist in providing experimental evidence for a nonuniform conduction-electron polarization, but will consist in describing the procedure we followed to unravel the complicated powder spectra. Barnes and Lunde[6] have reported their NMR results on $ScMn_2$, where one ^{45}Sc and two ^{55}Mn spectra give rise to a complex spectrum, from which they derive the various shift and quadrupole parameters. A complete account of their work has not yet been published, as far as we know, therefore we consider a description of a method to obtain all such information from a complex spectrum to be appropriate.

We obtained the quadrupole interactions of ^{11}B in the compounds RB_4 as a byproduct. It rendered us good service in separating the different spectra and determining the various shift parameters, but we shall not discuss the magnitudes of these quadrupole interactions. They may well fit into a series of papers on the theories of bonding in transition-metal boron compounds, from which we only mention a recent paper by Creel and Barnes.[7]

The report of this NMR investigation is organized as follows: In Sec. II we present the spin Hamiltonian and the theoretical treatment of the powder spectra. The NMR equipment and the preparation of the samples are given in Sec. III. Section IV contains a detailed description of the procedure we followed to determine the various shift and quadrupole parameters from the observed spectra, using the presentation of the theory given in Sec. II. The discussion in Sec. V is divided into two parts. In the first part the assignment of the different resonances to the three boron sites is justified, and the anisotropic part of the shifts is compared with the contribution from dipolar fields due to the rare-earth moments. In the second part an attempt is made to fit the obtained isotropic shifts within the RKKY scheme.

II. THEORY

The NMR spectrum of one particular boron site can be analyzed using the spin Hamiltonian

$$\mathcal{H} = \mathcal{H}_{\text{Zeeman}} + \mathcal{H}_{\text{sh}} + \mathcal{H}_Q , \tag{2.1}$$

where

$$\mathcal{H}_{\text{Zeeman}} = -\hbar\gamma_{\text{ref}}\,\vec{H}\cdot\vec{I} , \tag{2.2}$$

$$\mathcal{H}_{\text{sh}} = -\hbar\gamma_{\text{ref}}(K_z H_z I_z + K_x H_x I_x + K_y H_y I_y) , \tag{2.3}$$

and

$$\mathcal{H}_Q = \tfrac{1}{6}h\nu_Q[3I_z^2 - I(I+1) + \eta(I_x^2 - I_y^2)] . \tag{2.4}$$

$\mathcal{H}_{\text{sh}}$ represents the magnetic shift and $\mathcal{H}_Q$ stands for the nuclear quadrupole interaction. The axes x, y, and z are the principal axes of the electric-field-gradient (efg) tensor of the boron site in question. We assume that these axes coincide with the principal axes of the magnetic shift tensor. In Sec. V A we shall discuss the validity of this assumption for the three boron sites in a RB_4 crystal. H_x, H_y, and H_z are the components of the external static magnetic field $\vec{H}$. The quantity γ_{ref} is the gyromagnetic ratio of ^{11}B in a $Na_2B_2O_4$ solution[8] which is used as a reference for the magnetic shifts K_x, K_y, and K_z. In Eq. (2.4)

$$h\nu_Q = 3e^2qQ/[2I(2I-1)] , \tag{2.5}$$

where eq $(= V_{zz})$ and eQ have their usual meaning.[9,10]

Instead of working with K_x, K_y, and K_z, we prefer to use the isotropic shift K_{iso}, the axial shift K_z', and the asymmetry parameter ϵ, as defined by

$$\begin{aligned} &K_{\text{iso}} = \tfrac{1}{3}(K_x + K_y + K_z) , \\ &K_i' = K_i - K_{\text{iso}} \quad \text{for } i = x,\ y,\ \text{and } z , \\ &\text{and} \\ &\epsilon = (K_x' - K_y')/K_z' . \end{aligned} \tag{2.6}$$

It should be noted that the sequence of labeling

the axes x, y, and z is determined in the conventional way be requiring

$$|V_{zz}| \geq |V_{yy}| \geq |V_{xx}| \tag{2.7}$$

for the components of the efg tensor. The asymmetry parameter η in Eq. (2.4) is defined in the usual way by

$$\eta = (V_{xx} - V_{yy})/V_{zz}. \tag{2.8}$$

The condition (2.7) is equivalent to

$$0 \leq \eta \leq 1. \tag{2.9}$$

Our assumption that the principal axes of the magnetic shift tensor and of the efg tensor coincide does not imply any restriction for the value of the shift asymmetry parameter ϵ, such as Eq. (2.9) for η.

The shift and quadrupole parts [Eqs. (2.3) and (2.4)] of the Hamiltonian can be treated as a perturbation. In our case an adequate description of the experimental data is obtained if we carry terms up to first order for the shift and up to second order for the quadrupole interaction, while cross terms between shift and quadrupole interaction need not be considered. In the present NMR measurements the ν_Q values are usually less than 4% of the NMR frequency, and the K values are smaller than about 0.5%. The theory outlined in this section applies to any half-integer value of the nuclear spin I unless the restriction $I = \frac{3}{2}$ is explicitly mentioned. The direction of the external field $\vec{H}$ with respect to the axes x, y, and z will be characterized by the polar angles θ and φ where θ is the angle between the z axis and $\vec{H}$, and φ is the angle between the x axis and the projection of $\vec{H}$ on the xy plane. One then has the following expression for the resonance frequency $\nu_n(\theta, \varphi)$ of the transition $n + \frac{1}{2} \leftrightarrow n - \frac{1}{2}$ (n being integer)[11]:

$$\nu_n(\theta, \varphi) = \nu_R + \nu_{sh}^{(1)} + \nu_{nQ}^{(1)} + \nu_{nQ}^{(2)}, \tag{2.10}$$

where

$$\nu_{sh}^{(1)} = \nu_R [K_{iso} + \tfrac{1}{2} K_z' (3\mu^2 - 1 + \epsilon\kappa - \epsilon\kappa\mu^2)], \tag{2.11}$$

$$\nu_{nQ}^{(1)} = -\tfrac{1}{2} n \nu_Q (3\mu^2 - 1 + \eta\kappa - \eta\kappa\mu^2), \tag{2.12}$$

and

$$\nu_{nQ}^{(2)} = (\nu_Q^2/144\nu_R)[A(a_4\mu^4 + a_2\mu^2 + a_0) + B(b_4\mu^4 + b_2\mu^2 + b_0)]. \tag{2.13}$$

Here, the following abbreviations have been used:

$$\begin{aligned} &\nu_R = (\gamma_{ref}/2\pi)H, \quad \mu = \cos\theta, \quad \kappa = \cos 2\varphi, \\ &A = (I + \tfrac{3}{2})(I - \tfrac{1}{2}) - 3n^2, \\ &B = -8[(I + \tfrac{3}{2})(I - \tfrac{1}{2}) - 6n^2], \\ &a_4 = -b_4 = (3 - \eta\kappa)^2, \\ &a_2 = 2(-9 + 2\eta^2 - \eta^2\kappa^2), \\ &a_0 = (3 + \eta\kappa)^2, \\ &b_2 = 9 - \eta^2 - 6\eta\kappa + 2\eta^2\kappa^2, \\ &b_0 = \eta^2(1 - \kappa^2). \end{aligned} \tag{2.14}$$

These expressions or parts of them can be found in several papers[7,10,12-15] but one should note that some authors[7,10,12,14] use a different angle φ, which makes κ change sign.

Our experimental data are on polycrystalline samples only and we are therefore interested in the so-called powder patterns, which can be constructed theoretically using Eq. (2.10) and varying θ and φ to cover all possible orientations of $\vec{H}$ with respect to the set of axes x, y, and z. In the general case of both quadrupole interaction and magnetic shift, the integration that has to be performed in order to obtain the powder pattern cannot be carried out analytically. One should therefore integrate numerically, using a digital computer. However, particular features of the powder pattern, such as the frequencies of peaks and shoulders, can be expressed in an analytical form. An extensive treatment of the features of powder patterns in the case of a completely asymmetric shift and quadrupole interaction is given by Baugher, Taylor, Oja, and Bray.[14] We shall quote from this paper while making a small extension of the theory; i.e., we shall always take account of the second-order quadrupole perturbation term [Eq. (2.13)], whereas Baugher *et al.* used this term only for the central line ($n = 0$).

In the RB_4 compounds, the central transitions of the three lattice sites strongly overlap and it is not possible to identify peaks or shoulders. We shall therefore not dwell on the theoretical powder pattern of the central transition.

The other transitions ($n \neq 0$), usually called satellites, will be treated now. Figure 1 gives the absorption and derivative patterns of one single transition $n + \frac{1}{2} \leftrightarrow n - \frac{1}{2}$. Details of this figure will be treated when discussing the computer calculations. In the figure, the first-order quadrupole splittings are assumed to dominate the magnetic shifts. (If this were not so, satellites would not be observable because they would vanish under the central transition absorption.) The absorption shows a shoulder at $\nu_6 - \nu_R$ corresponding to $\theta = 0°$. The shoulder at $\nu_2 - \nu_R$ and the peak at $\nu_3 - \nu_R$ correspond to the combinations $\theta = 90°$ with $\varphi = 90°$, and $\theta = 90°$ with $\varphi = 0°$, respectively. As long as the second-order quadrupole perturbation is small, its consideration does not, in general, modify the theoretical shape discussed by Baugher *et al.*[14] The frequencies of the shoulders and peaks in Fig. 1 are

$$\nu_2 = \nu_R[1 + K_{iso} - \tfrac{1}{2} K_z'(1 + \epsilon)] + \tfrac{1}{2} n \nu_Q (1 + \eta) + A\nu_Q^2 (1 - \tfrac{1}{3}\eta)^2/16\nu_R,$$

$$\nu_3 = \nu_R[1 + K_{iso} - \tfrac{1}{2}K'_z(1-\epsilon)] + \tfrac{1}{2}n\nu_Q(1-\eta) + A\nu_Q^2(1+\tfrac{1}{3}\eta)^2/16\nu_R, \quad (2.15)$$

$$\nu_6 = \nu_R(1 + K_{iso} + K'_z) - n\nu_Q + A\nu_Q^2\eta^2/36\nu_R,$$

where A is given in Eqs. (2.14).

The addition of second-order terms may give rise to an extra shoulder or peak, which is, however, of no practical interest. It can only occur if ν_2 and ν_3 come extremely close together, which happens if $n\eta\nu_Q$ and $\epsilon K'_z\nu_R$ almost cancel.

Our experimental data refer to ^{11}B nuclei, for which $I = \frac{3}{2}$. For $I = \frac{3}{2}$, the situation is simplified considerably, since there is only one pair of satellites ($n = +1$ and $n = -1$) and since $A = 0$ [see Eqs. (2.14)], making the second-order perturbation zero at the position of the shoulders and peaks in the powder pattern. One should note, however, that the second-order term is not zero for intermediate angles θ and φ. It may play a role in the shape of the powder pattern.

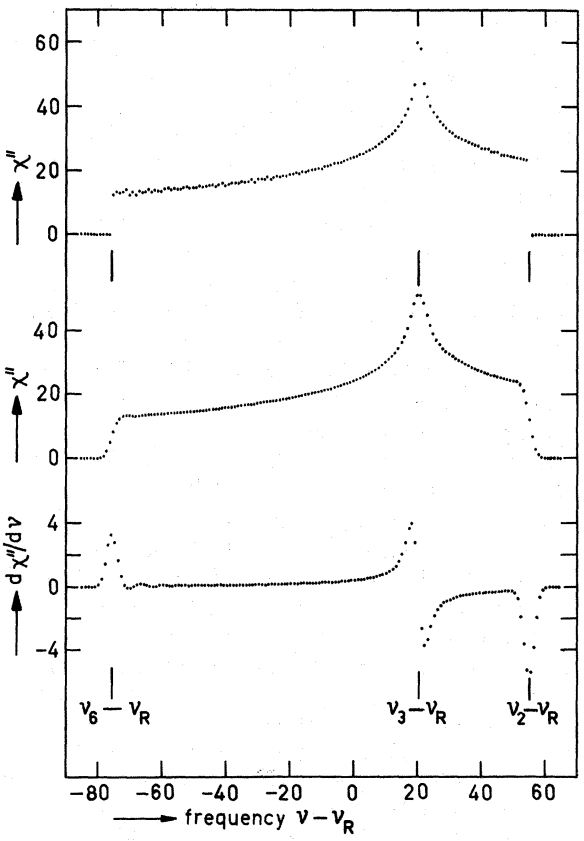

FIG. 1. Powder pattern of one satellite transition $n + \frac{1}{2} \longleftrightarrow n - \frac{1}{2}$. The upper curve gives the absorption without line broadening. The middle and lower curves give the broadened absorption and derivative. The dots are obtained from a computer calculation. The vertical scales are in arbitrary units. Horizontally, channel numbers are given, as used in the computer calculation.

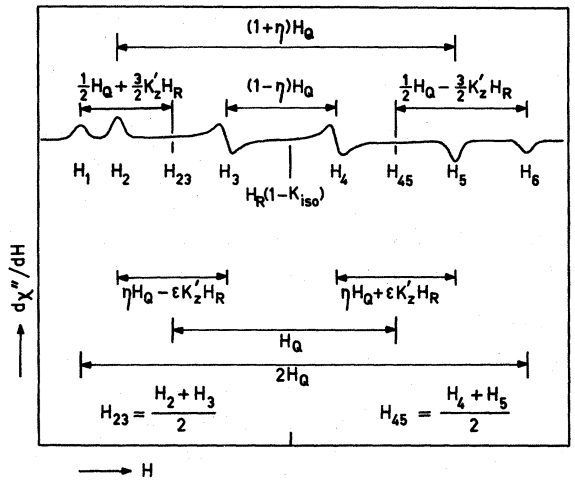

FIG. 2. Absorption derivative powder pattern of both satellite transitions $n + \frac{1}{2} \longleftrightarrow n - \frac{1}{2}$, $n = +1$ and $n = -1$, for $I = \frac{3}{2}$. Expressions for H_1 through H_6 are given by Eqs. (2.17). Intervals determining the various spin-Hamiltonian parameters are indicated. The figure is drawn for $K'_z < 0$ and $\epsilon < 0$.

Figure 2 gives the powder pattern of both satellites for $I = \frac{3}{2}$. This figure is adapted to the experimental situation where the frequency ν is fixed and the external field is varied. The special points occurring at H_2, H_3, and H_6, respectively, correspond to those at ν_2, ν_3, and ν_6 in Fig. 1. The relation between a resonance frequency $\nu(\theta, \varphi)$ at a field H_R and a resonance field $H(\theta, \varphi)$ at a frequency $\gamma_{ref} H_R/2\pi$ $(= \nu_R)$ may be approximated by

$$\nu(\theta, \varphi) - \nu_R = -(\gamma_{ref}/2\pi)[H(\theta, \varphi) - H_R]. \quad (2.16)$$

The error made in this approximation is of third order in the quadrupole interaction and of the order of cross terms between shift and quadrupole interaction. Both types of terms were neglected earlier so that Eq. (2.16) holds within the frame of approximations used in Eq. (2.10). We obtain the following expressions for the shoulders and peaks for $I = \frac{3}{2}$, as indicated in Fig. 2:

$$\begin{aligned} H_1 &= H_R(1 - K_{iso} - K'_z) - H_Q, \\ H_2 &= H_R[1 - K_{iso} + \tfrac{1}{2}K'_z(1+\epsilon)] - \tfrac{1}{2}H_Q(1+\eta), \\ H_3 &= H_R[1 - K_{iso} + \tfrac{1}{2}K'_z(1-\epsilon)] - \tfrac{1}{2}H_Q(1-\eta), \\ H_4 &= H_R[1 - K_{iso} + \tfrac{1}{2}K'_z(1-\epsilon)] + \tfrac{1}{2}H_Q(1-\eta), \\ H_5 &= H_R[1 - K_{iso} + \tfrac{1}{2}K'_z(1+\epsilon)] + \tfrac{1}{2}H_Q(1+\eta), \\ H_6 &= H_R(1 - K_{iso} - K'_z) + H_Q, \end{aligned} \quad (2.17)$$

where

$$H_Q = \nu_Q/(\gamma_{ref}/2\pi). \quad (2.18)$$

For the discussion of the experimental results, it is convenient to introduce

$$H_{23} = \tfrac{1}{2}(H_2 + H_3) = H_R(1 - K_{iso} + \tfrac{1}{2}K'_z) - \tfrac{1}{2}H_Q$$

and (2.19)

$$H_{45} = \tfrac{1}{2}(H_4 + H_5) = H_R(1 - K_{iso} + \tfrac{1}{2}K'_z) + \tfrac{1}{2}H_Q$$

In Fig. 2, intervals are given determining the various spin-Hamiltonian parameters.

The computer calculations of powder patterns were performed in a manner described by various authors, for example by Narita, Umeda, and Kusumoto[13] and by Baugher *et al.*[14] First, the lowest and highest frequency of the powder pattern are calculated. Then the range of frequencies between these two extremes (or a somewhat larger range) is divided in N equal intervals, N being of the order of 100. These intervals will be called frequency channels. Next, μ ($=\cos\theta$) and φ are scanned over a large number of equally probable values. For each combination of values for μ and φ, the frequency of resonance is calculated, using Eq. (2.10). Then one count is added to the corresponding frequency channel. In practice we have chosen the values $(n-\frac{1}{2})\mu_{step}$ $(n=1, 2, \ldots, N_\mu)$ for μ, where $\mu_{step} = 1/N_\mu$, and similarly the values $(n-\frac{1}{2})\varphi_{step}$ $(n=1, 2, \ldots, N_\varphi)$ for φ, where $\varphi_{step} = \frac{1}{2}\pi/N_\varphi$. Usually, N_μ and N_φ were both chosen as 300, but for small values of η, smoother curves were obtained by taking a larger value for N_μ and a smaller value for N_φ, the product $N_\mu \times N_\varphi$ being kept constant. The upper curve in Fig. 1 gives an example of the contents of the channels (in arbitrary units) as a function of channel number. The next step is a convolution with a Gauss function

$$e^{-(\nu-\nu')^2/2\sigma^2}, \qquad (2.20)$$

resulting in a curve like the middle one in Fig. 1. Finally, the derivative is determined by simply taking the differences between the contents of two adjacent channels. This is illustrated in the lower part of Fig. 1.

The complete program can be used for any transition $n+\frac{1}{2} \leftrightarrow n-\frac{1}{2}$, $n = -I+\frac{1}{2}, -I+\frac{3}{2}, \ldots, 0, \ldots, I-\frac{1}{2}$, and for any half-integer value of the spin I. The absorption for each transition is multiplied by the transition probability factor $(I+\frac{1}{2}+n)(I+\frac{1}{2}-n)$. The patterns of the various transitions can be plotted automatically, either separately or summed.

III. EXPERIMENTAL

The samples RB_4 (R = La, Nd, Gd, Ho) were prepared by arc melting using starting materials of 99.9% purity (R) and 99.99% purity (B). The presence of second phases was checked by x-ray diffraction. The compound LaB_4 proved to be not of a single phase after arc melting and a special treatment, described in detail in Ref. 16, was needed. NMR experiments were carried out on powdered samples, screened through a 50-μm sieve.

Our NMR spectrometer is a coaxial version of the "reflection-cavity"-type EPR instrument and combines several features of earlier published spectrometers.[17,18] We shall describe this setup in some detail.

The rf power source is a Hewlett–Packard (HP) 606B oscillator, which is stabilized with a HP 8708A synchronizer. It is followed by a simple series resonant circuit to remove unwanted higher harmonics, and by stepped attenuators (HP 355C and 355D: 132 dB in 1-dB steps) for saturation studies. Since no circulators in the frequency range of interest (4–30 MHz) are available, we used a 17-dB directional coupler (Anzac CNJ-7940) instead of the more frequently employed magic tee.[17] With this choice, we lose 14 dB of transmitter power but gain a low-loss (0.2 dB) path from the "cavity" to the receiver compared to a setup with a magic tee. The parallel resonant circuit containing the NMR sample is connected to the directional coupler by means of a small series capacitor, the value of which is kept just below critical coupling. Both tuning and coupling capacitors are located in a brass box on top of the cryostat. A rigid coaxial air line, made of stainless steel, connects the sample coil with the capacitors. Two control loops maintain phase and amplitude balance. The control circuits are quite similar to those of Mehring and Kanert.[18] The transistorized broadband receiver of conventional design was built in our laboratory. It is followed by a diode detector, lock-in amplifier, and recorder.

The magnetic field (up to 16 kG) is provided by a Varian 12-in. magnet. Field modulation is usually at 80 Hz. The fields are measured with an AEG proton-NMR field-measuring instrument. With a counter the field is displayed directly in gauss, by dividing the proton frequency by 42.5759 kHz from a fixed quartz oscillator (Rohde & Schwarz). The same counter is used to monitor the frequency of the rf power source.

When more than about one hour of recording time is necessary to obtain a reasonable signal-to-noise ratio, we use a time-averaging computer.[19] With the field dial in the "sawtooth" mode, we derive a pulse from the proton-absorption line to trigger the time-averaging computer, which then runs freely on its own clock. Usually the sweep time (for a single sweep) is 10 min, while the computer runs through its 400 channels in 8 min. The field value at which triggering occurs is kept within ± 0.1 G for long periods of time: A home-made synchronizer enables us to lock the proton frequency to a harmonic of the quartz oscillator (42.5759 kHz), thus providing us with highly stable proton frequencies at intervals equivalent to 10 G. The stability of the whole spectrometer readily allows overnight operation.

IV. RESULTS

A. Crystal Structure

The crystal structure of the RB_4 compounds[20] is tetragonal, space group $P4/mbm$ (Schoenflies D_{4h}^5). There are four formula units RB_4 per unit cell. The four R atoms are on a site having point symmetry $mm2$. Boron atoms occur at three different sites:

4 boron atoms at site $4e$, point symmetry 4,

8 boron atoms at site $8j$, point symmetry m,

4 boron atoms at site $4h$, point symmetry $mm2$.

The upper part of Fig. 3 gives a projection of the atoms on a plane perpendicular to the tetragonal or c axis. The boron atoms $8j$ and $4h$ are situated $0.5c_0$ above the basal plane, c_0 being the cell edge in the c direction. The height of the other atoms is indicated in the figure. The values of the cell edges of NdB_4 are[16,20,21] (rounded off to 3 digits) $a_0 = 7.22$ Å and $c_0 = 4.10$ Å. The lower part of Fig. 3 gives a projection along one of the a axes, some atoms being left out for the sake of clearness.

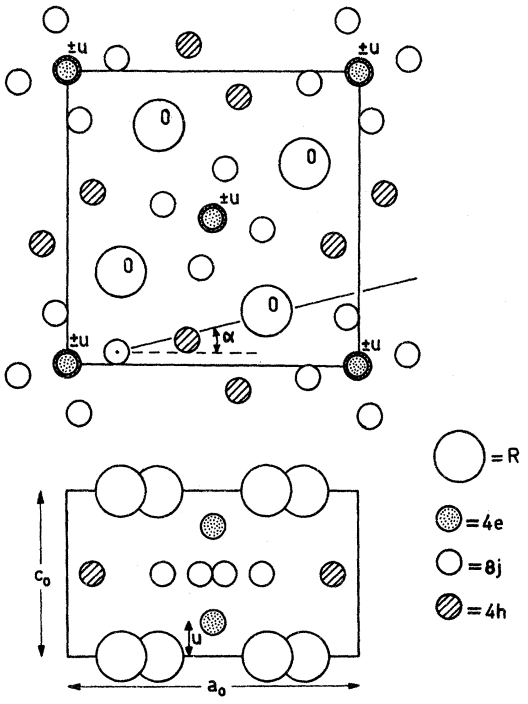

FIG. 3. Crystal structure of RB_4. The three boron sites are denoted by $4e$, $8j$, and $4h$. The upper part gives a projection along the tetragonal c axis. For R and for boron $4e$, the height above the basal plane is indicated; for the other boron atoms ($4h$ and $8j$), this height is $0.5c_0$. The lower part gives a projection along one of the a axes, some atoms being omitted for clearness. More details can be found in Ref. 20.

B. LaB_4

The upper trace in Fig. 4 represents a recording of the ^{11}B resonance at 4.2 K. The second one is a computer-simulated fit to the experiment, using the parameters listed in Table I. The $n=0$ ($\frac{1}{2} \leftrightarrow -\frac{1}{2}$) transitions have been omitted in the simulations and will be treated separately. The simulated spectrum is the sum of three simple spectra, labeled $4e$, $8j$, and $4h$, which represent the contributions of the three boron sites.

We shall now treat the determination of the parameters in detail and discuss the assignment of each of the three simple spectra to a particular boron site.

Confronted first with the experimental spectrum, it seems rather obvious to start the analysis with the sharp peaks at 12.99 and 13.24 kG. For the sake of completeness we recall, at this point, that for axial symmetry our prototype spectrum of Fig. 2 transforms into the well-known form of trace "$4e$" in Fig. 4. In that case, the special points H_2 and H_3 merge into the so-called 90° satellite ($\theta = 90°$) at H_{23}, and similarly H_4 and H_5 become one line at H_{45}. (The $\theta = 0°$ satellites are always at H_1 and H_6 and hardly change their intensity.) Returning to the experimental spectrum, we want to interpret these peaks as 90° satellites of the only axially symmetric site $4e$ in the LaB_4 crystal. This immediately provides us with the value of the quadrupole interaction $H_Q = H_{45} - H_{23}$. We obtain $H_Q = 251(3)$ G, the number in parentheses indicating the estimated uncertainty in the preceding digit. The separation between the 0° satellites is now prescribed to be $2H_Q$ and so they can easily be located in the experimental spectrum. These peaks are rather weak in Fig. 4 but we obtained better signal-to-noise ratios in separate recordings of small parts of the spectrum. Once their positions are known (H_1 and H_6 in Fig. 2), we can easily solve Eqs. (2.17) to obtain the parameters $K_{iso} = 0.00(2)\%$ and $K_z' = 0.00(3)\%$ for site $4e$.

We wish to stress here that knowledge of the 90° satellites only is not sufficient to obtain both K_{iso} and K_z'. At least one 0° satellite must also be observable. The abundant information contained in the position of the other 0° satellite can be of great help in locating them both: No other pair of equal-intensity peaks with the prescribed separation ($2H_Q$) can be found in the experimental spectrum. Of course the same argument holds when, for instance, the 0° satellites are clearly observable and the position of only one of the 90° satellites can be determined, a situation which we shall encounter in discussing the 77-K spectra of NdB_4.

To complete the discussion of site $4e$ we finally estimate the value of the broadening parameter σ [Eq. (2.20)] from the width of the 90° satellites,

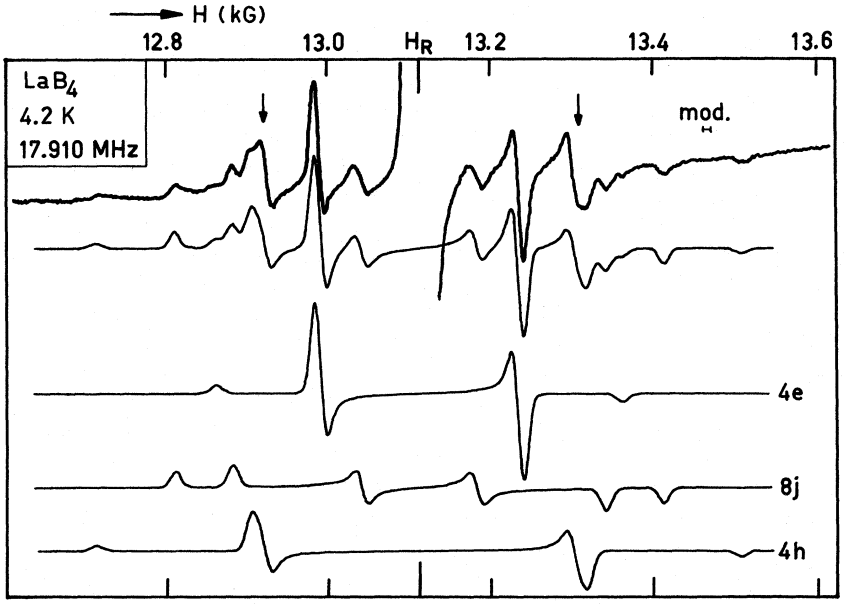

FIG. 4. Measured absorption derivative satellite spectrum (upper trace) of ^{11}B in polycrystalline LaB_4 at 4.2 K and 17.910 MHz. The measuring time was 50 min (one scan) and the modulation was 10 G peak to peak. The second curve gives the computer-simulated spectrum, the central transition being left out. The three lower curves represent the contributions of boron atoms at the sites $4e$, $8j$, and $4h$. The parameters used in the simulated spectra are those of Table I. The two arrows mark the positions of the 90° satellite peaks of ^{11}B in LaB_6. The resonance field of the reference compound $Na_2B_2O_4$ is denoted by H_R.

using computer-simulated spectra. We obtain $2\pi\sigma/\gamma_{ref} = 6.4$ G. We shall use the broadening parameter mainly to optimize the fit of the simulated curves to the experiment, not attempting to give a complete discussion of the contributions to σ. Besides dipolar interaction among the nuclei, inhomogeneous broadening due to a distribution of efg values may be present. Moreover, in paramagnetic compounds like NdB_4 (Secs. IV C and IV D) a distribution of Knight shifts and also demagnetization fields will cause inhomogeneous broadening.

We now focus our attention on the outermost peaks in the spectrum of LaB_4 at 12.72 and 13.51 kG. We suppose them to be 0° satellites of one of the three boron sites, which we shall call $4h$ for ease of presentation. We shall account for the real assignment of these peaks to site $4h$ later on.

From their separation one obtains $H_Q = 398(3)$ G and, using this value, the location of the corresponding 90° points H_{23} and H_{45} in the experimental spectrum is simplified. Since we have already assigned a set of satellites to the only axially symmetric site ($4e$), we must now take into account the possibility of nonzero values for η and ϵ [Eq. (2.17)]. The points H_{23} and H_{45} are found to be somewhere in the middle of the broadened peaks at 12.91 and 13.31 kG; apparently the peaks corresponding to the special points H_2 and H_3 strongly overlap and information about η and ϵ can only be obtained from the width of their resultant, which we shall call again H_{23}. The same holds for H_4, H_5, and H_{45}. From the separations $H_{23} - H_1$ and $H_6 - H_{45}$ we conclude that $K'_z = 0.00(2)\%$. The width of H_{23} and H_{45} is now only dependent on η and on

TABLE I. Results of ^{11}B NMR measurements in LaB_4 and NdB_4.

	Site	Point symmetry	ν_Q (kHz)	H_Q (G)	η	K_{iso} (%)	K'_z (%)	ϵ	$2\pi\sigma/\gamma_{ref}$ (G)
LaB_4 at 4.2 K[a]	$4e$	4	343(4)	251(3)	0	0.00(2)	0.00(3)	...	6.4
	$8j$	m	412(4)	302(3)	0.53(1)	0.00(2)	0.00(2)	...	
	$4h$	$mm2$	544(4)	398(3)	0.045(20)	0.00(2)	0.00(2)	...	
NdB_4 at 77 K[b]	$4e$	4	420(6)	307(4)	0	+0.33(3)	−0.36(4)	0	9.1 at 18 MHz and 7.3 at 9 MHz
	$8j$	m	443(10)	324(8)	0.51(2)	+0.26(4)	−0.30(6)	−0.4(2)	
	$4h$	$mm2$	622(6)	455(4)	<0.05[c]	+0.23(3)	+0.34(4)	$\gtrsim 0$[c]	

[a]Within the experimental accuracy, the values of ν_Q and η are found to be independent of temperature in the range 4–300 K.

[b]At room temperature, the observed spectrum can be described well (Fig. 5) using the same values for ν_Q, η, and ϵ, but smaller values for K_{iso} and K'_z, in proportion to the susceptibility. For the broadening parameter we used $2\pi\sigma/\gamma_{ref} = 7.3$ G.

[c]Computer simulations have been performed using $\eta = 0.02$ and $\epsilon = +0.2$.

the broadening parameter σ, since ϵ has a minor influence. In order to obtain a reasonable value for η from these peaks, we studied the width of H_{23} as a function of η and the broadening parameter σ. Although one cannot obtain a unique pair of values for σ and η from a single experimental width, upper limits can generally be given. Using the same value for σ as in the simulated spectrum for $4e$, where it can be obtained more rigorously because $\eta = \epsilon = 0$, we find $\eta = 0.045(20)$, while in any case $\eta < 0.065$ (this value is reached for $\sigma \to 0$). The positions of the different special points now being known, it is a straightforward matter to obtain for $4h$ $K_{iso} = 0.00(2)\%$.

With these parameters the simulated $4h$ spectrum does not follow the experimental trace completely, some intensity being missed at the "inner" sides of the 90° satellites. We ascribe this deviation to a small amount of a second phase: LaB_6. We prepared and measured this phase separately and found a value of $H_Q = 380(4)$ G for ^{11}B in LaB_6, in agreement with the results of Gossard and Jaccarino.[22] The precise locations of the peaks of the 90° satellites of LaB_6 (boron is at a site of axial symmetry in this compound) are indicated in Fig. 4 by small arrows at 12.921 and 13.309 kG. (Computer spectra show that the H_Q value is slightly smaller than the peak separation of 388 G.) Comparison of intensities led us to an estimated concentration of 3–4 wt% LaB_6. One should bear in mind here that in LaB_6 all borons are equivalent, so in first approximation one unit of LaB_6 produces a boron resonance six times stronger than the $4h$ boron in a unit LaB_4. Indications of the presence of this second phase were also found in the x-ray diagrams.

From the remaining peaks in the spectrum, which of course are to be ascribed to the remaining boron site—we shall call this one $8j$ in advance—we interpret the peaks at 12.81 and 13.41 kG as 0° satellites, providing us with $H_Q = 302(3)$ G for $8j$. This is justified by the possibility of finding the corresponding 90° positions in the spectrum: taking the peaks at 12.88 and 13.34 kG as H_2 and H_5, and assigning the zero crossings at 13.04 and 13.18 kG to H_3 and H_4, the separation between H_{45} and H_{23} agrees nicely with the already determined value of H_Q. The other parameters turn out to be: $\eta = 0.53(1)$, $K_{iso} = 0.00(2)\%$, and $K'_z = 0.00(2)\%$, ϵ being undetermined.

We are now in a position to discuss the assignment of the simple spectra to the sites $4h$ and $8j$. Although we are aware of the caution with which one should handle intensity arguments, the impossibility of an interchange in the assignment to $4h$ and $8j$ can be based upon such arguments without doubt. In the computer simulations in Fig. 4, we took into account the double occurrence of $8j$ with respect to $4h$ and $4e$. If one were to attempt to interpret the experimental spectrum with the assignments $4h$ and $8j$ interchanged, one should reduce the amplitude of trace $8j$ by a factor of 2, and at the same time double the amplitude of $4h$. If this is done, the intensity ratio between the peaks of $4h$ and $8j$ changes by a factor of 4. As the intensity ratios in the simulated spectrum with the tentative assignment agree excellently with experiment, we reject an interchange of $4h$ and $8j$. Another point should be discussed here: Since the value of η of site $4h$ turns out to be close to zero, one could think of interchanging $4e$ and $4h$ by letting their broadening parameters differ appreciably. Although we cannot here rule out this possibility completely, we consider it to be very improbable, and we will find strong evidence against it when discussing the origins of shift anisotropy in NdB_4 (Sec. V).

The central ($n = 0$) transitions of the three sites almost coincide. The linewidth (separation between absorption derivative extrema) is 13.2 G at 13 kG. To find the true center of the experimental line, we used the values of the quadrupole interaction, obtained from the $n = \pm 1$ transitions, to simulate a (second-order-broadened) central line. We obtained $K_{iso} = 0.00(1)\%$, which is in agreement with the data derived from the satellites.

To conclude our presentation of experimental results on LaB_4, we make two remarks: (i) We did not attempt to determine T_1 values, but took care to record our spectra with sufficiently low values of the rf magnetic field, since we could clearly observe saturation effects; (ii) within the experimental error neither the shifts nor the quadrupole interactions revealed any temperature dependence (4–296 K).

C. NdB_4 at 296 K

To give an outline of the method we used to analyze our spectra, we have treated the determination of the various parameters of LaB_4 very thoroughly. For NdB_4 we followed essentially the same procedure, so we shall not give a complete discussion once again, but dwell on some critical steps only. We carried out measurements on NdB_4 at room temperature and at 77 K.

The room-temperature spectrum is given in Fig. 5. It has much in common with the LaB_4 spectrum in Fig. 4. In LaB_4, the sequence of quadrupole interaction strengths (H_Q values) is $4e$-$8j$-$4h$ and since the c_0/a_0 ratios of LaB_4 and NdB_4 do not differ much (they are 0.571 for LaB_4 and 0.568 for NdB_4[16,20,21]), we shall assume that this sequence does not change, when passing from LaB_4 to NdB_4. This solves the assignment problem and again the lower traces represent the simple spectra of the three boron sites.

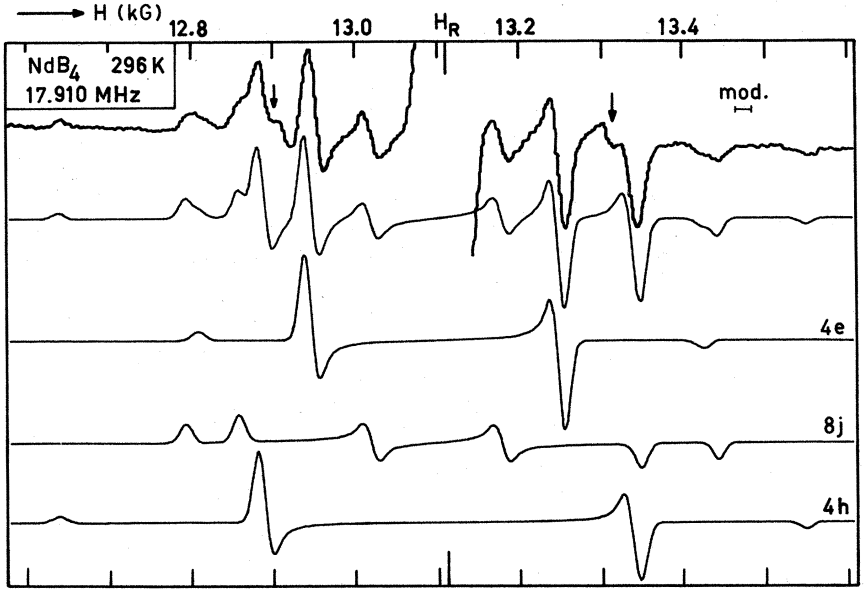

FIG. 5. Measured (upper curve) and simulated (lower curves) derivative satellite spectra of ^{11}B in polycrystalline NdB_4 at 296 K and 17.910 MHz. The low-field ($H < H_R$) and high-field parts of the spectrum were each obtained from 92 scans of 10 min (2×15.3 h). The modulation was 20 G peak to peak. The parameters used in the simulated spectra are those of Table I. The two arrows mark the positions of the 90° satellite peaks of ^{11}B in NdB_6.

For site 4*e* we obtain $H_Q = 307(4)$ G from the separation of the 90° satellites. The 0° satellites of 4*h* provide us with $H_Q = 455(4)$ G. The asymmetric humps at 12.80 and 13.45 kG contain the 4*e* 0° satellites (prescribed separation) at their "inner" sides (i.e., towards the center of the spectrum), the outer contribution being the 8*j* 0° satellites, which should be roughly twice as strong. With a fixed separation for the 4*e* 0°'s, we could determine the 0°–90° distance within ± 6 G, yielding $K'_z = -0.11(3)\%$. The 8*j* 0°'s fix the quadrupole interaction for 8*j* at $H_Q = 324(8)$ G. Next, we determined the separation between the special points H_3 and H_4 for 8*j*: $(1-\eta)H_Q = 158(3)$ G, so $\eta = 0.51(2)$, the error in η mainly resulting from the uncertainty in the H_Q value for 8*j*.

The humps between the 0° and 90° satellites of 4*e* need some more discussion: They contain 90° peaks of both 4*h* and 8*j*. Moreover, at the inner side of these humps there are small peaks, which one does not find in the simulated spectrum. We shall deal with them first: They are 90° satellites of a small amount (approximately 3 wt% from intensity considerations) of a second phase, NdB_6, which we studied separately, just like LaB_6. The small arrows in Fig. 5 indicate the position of the peaks of the 90° satellites of ^{11}B in NdB_6. In the low-field hump, the shoulder at 12.86 kG stems from the special point H_2 of site 8*j*, which follows from the fact that: (i) the separation H_2-H_5 is fixed by the values of H_Q and η, $H_Q(1+\eta) = 489(12)$ G; (ii) the intensities of peak and shoulder agree quite well with the simulated spectra, which they do not if one tries to interpret the shoulder as the special point H_2 of 4*h*. At the high-field side, the point H_5 of 8*j* coincides with the 4*h* 90° satellite. Without knowledge of H_5 we are still able to obtain for 8*j*: $K'_z = -0.10(5)\%$, $\epsilon = -0.5(6)$.

For 4*h* the 90° points H_{23} and H_{45} are now readily determined, with which we obtain $K'_z = 0.09(3)\%$. From the widths of H_{23} and H_{45}, an upper limit of 0.05 for η can be estimated, while ϵ again remains undetermined.

Concerning the isotropic shifts, we can remark that differences in shift for the three boron sites at room temperature are hidden completely in the experimental errors. The whole spectrum is shifted with respect to our reference compound ($Na_2B_2O_4$) by $K_{iso} = +0.04(3)\%$.

D. NdB_4 at 77 K

We now discuss the spectra of NdB_4, taken at 77 K. The first one, at the same frequency as the room-temperature spectrum (17.910 MHz), is presented in Fig. 6. Compared with the situation at room temperature, things have now changed drastically. First, one observes that the center of the spectrum is shifted clearly towards lower field values with respect to the reference field H_R. Secondly, the symmetry of the spectrum is very much reduced, pointing to appreciable anisotropic contributions to the shifts. In order to be able to unravel this spectrum, we need more information. We find it in a 77-K spectrum at 8.955 MHz (Fig. 7), which can be considered as an intermediate case between the now familiar 296-K spectrum and the 77-K one at 17.910 MHz.

Another valuable source of information is contained in spectra on aligned samples: When first recording 77-K spectra of NdB_4, we observed rather unusual intensity ratios between 0° and 90° satellites, while with no precautions being taken

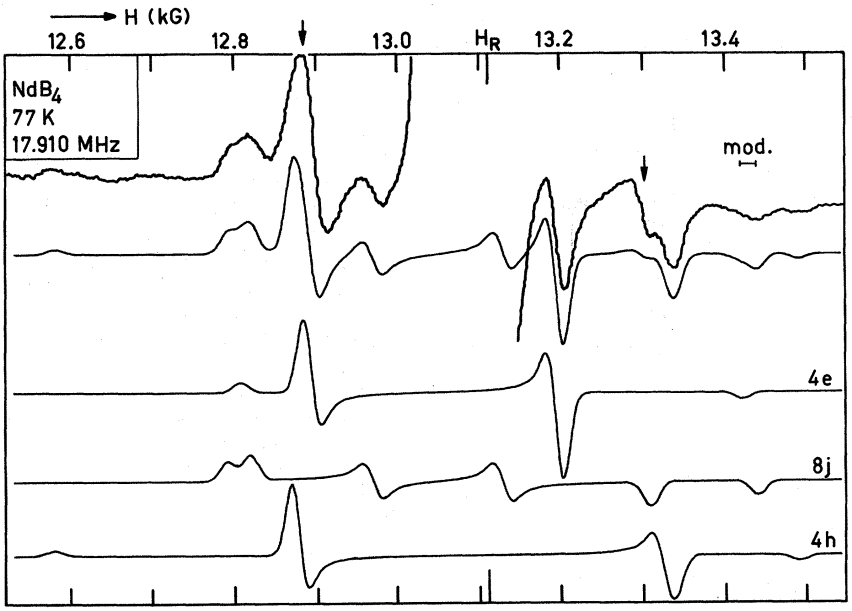

FIG. 6. Same spectrum as Fig. 5 (NdB_4, 17.910 MHz), but now at a temperature of 77 K. The measuring time was 8 h.

the room-temperature spectra were correct in this respect. We would ascribe these anomalies to an appreciable anisotropy of the static magnetic susceptibility, which in turn causes the grains to become aligned by the magnetic field, leaving us with a partially textured sample. At room temperature, these effects are apparently too small to cause any texture: (i) The susceptibility is lower by roughly a factor of 4; (ii) the difference $\chi_{\parallel} - \chi_{\perp}$ is probably lowered even more than this factor because of disappearing crystal field effects. We dealt with this matter in two ways: (i) We prepared a sample by freezing it in ethanol at zero field to retain a "real powder"; in fact the spectra of Fig. 6 and 7 are taken on such a sample. (ii) We tried to enlarge the spurious alignment by deliberately orienting the powder at liquid-helium temperatures and high fields, and then, without moving anything, we recorded a 77-K spectrum which is shown in Fig. 8. The differences between the latter and Fig. 6 are striking. They will supply important information both on the analysis of the 77-K spectra and on the interpretation of the experimental data.

Comparing now Figs. 6 and 8 in some detail, we notice that the strong 90° peaks of both 4*e* and 4*h* at low and high fields have almost disappeared in

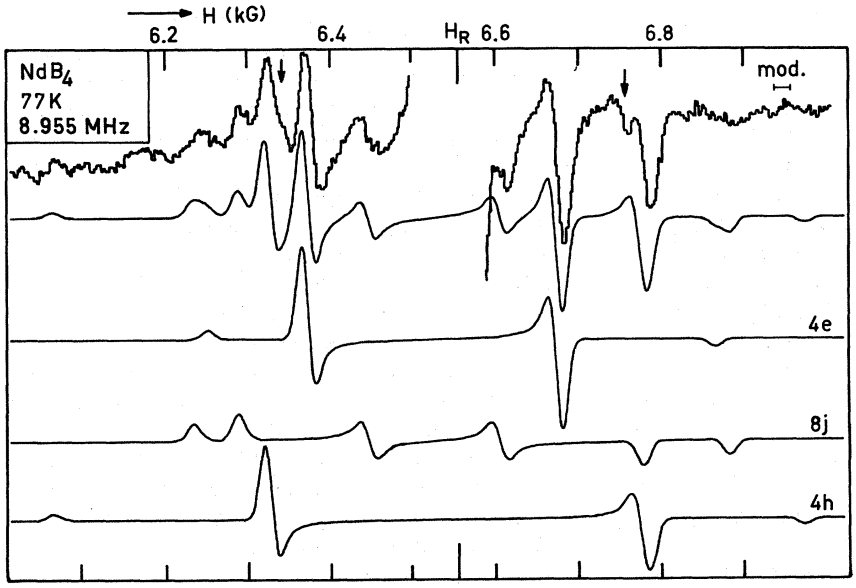

FIG. 7. Same spectrum as Fig. 6, but now at 8.955 MHz. The measuring time was 19 h.

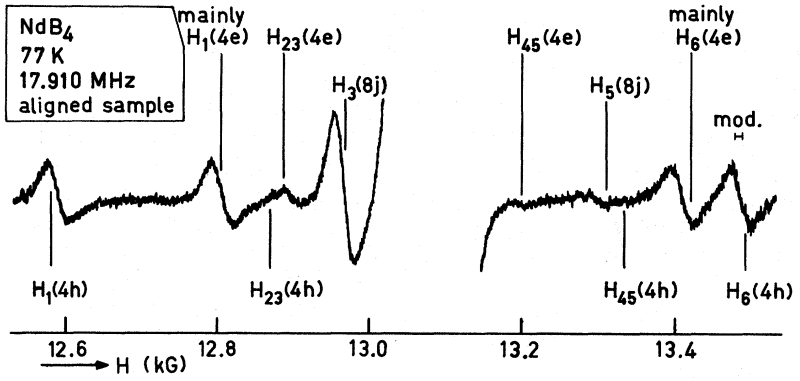

FIG. 8. Same spectrum as Fig. 6 (17.910 MHz, 77 K), but now the powder particles are substantially aligned by the applied field $\vec{H}$ due to the anisotropy of the susceptibility. In Figs. 6 and 7 such an alignment is artificially prevented. The measuring time was 100 min (one scan) and the modulation was 10 G peak to peak.

the spectrum of the aligned sample, while their 0° satellites are now very strong. On the other hand, the peak corresponding to the special point $H_3(\theta = 90°, \varphi = 0°)$ of the site 8*j* has increased strongly in the aligned sample, whereas the satellite at $H_5(\theta = 90°, \varphi = 90°)$ is relatively weak, and the 0° satellites of 8*j* have probably also become very weak in Fig. 8. We shall draw an important conclusion from these data: From the gain in intensity of the 0° satellites of 4*e*, we conclude that the *c* axes of the grains are turned towards the field direction. This follows directly from the fact that the *z* axis of the efg tensor (see Sec. II) coincides with the uniaxial symmetry axis (*c* axis) of the 4*e* site. In terms of the static susceptibility this conclusion can be simply stated as $\chi_{\parallel} > \chi_{\perp}$. From the similar behavior of the satellites of 4*h*, the *c* direction must also coincide with the *z* axis of 4*h*. We remark that this *z* axis is apparently not along the twofold symmetry axis of 4*h*, which lies in the plane perpendicular to the *c* axis. The *z* axis of site 8*j* is found to lie in the plane perpendicular to the *c* direction, while of course one of the principal directions of 8*j* is still the *c* direction for symmetry reasons. This will be discussed further in Sec. V A.

At this point we shall confine ourselves to presenting Table I, which gives the various parameters obtained from the spectra. We wish to emphasize here that, for NdB_4, essentially only one set of parameters was used to fit both room-temperature and 77-K spectra, the shifts being proportional to the susceptibility.[16] A minor point should be noted: The broadening parameter σ in the 77-K spectrum at 17.910 MHz (Fig. 6) was $2\pi\sigma/\gamma_{ref} = 9.1$ G; this somewhat higher value, compared with $2\pi\sigma/\gamma_{ref} = 7.3$ G in the other NdB_4 spectra, accounts for increased inhomogeneous broadening.

It has been mentioned already in Secs. I and II that the central transitions of the three boron sites overlap to a considerable extent. Therefore, one could never determine all the given parameters from experiments on this transition only. However, it is useful to compare an experimental trace with a computer simulation, using the parameters obtained from the satellites. This is done in Fig. 9 at 77 K and 17.910 MHz. Generally, the agreement is satisfactory, but a deviation can be seen in the form of a long tail at the high-field side. We have no precise explanation for this effect. Qualitatively, the origin could be some free boron in the sample, but the amount of it needed to explain the deviation entirely seems rather large. Further, there are slight contributions from the second-phase NdB_6 and from the satellite $H_4(8j)$ of NdB_4, which is at 13129 G; we found that these two effects alone are again too small to explain the

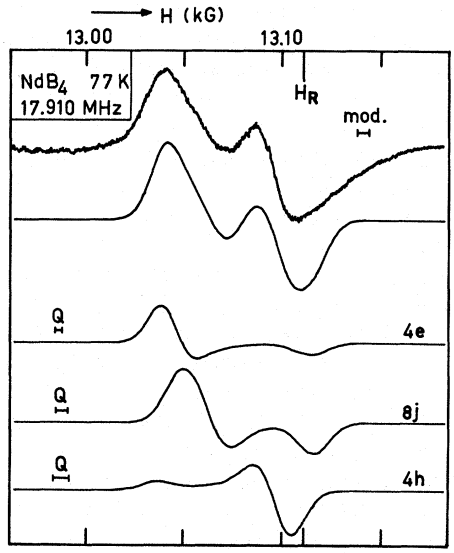

FIG. 9. The central transition of ^{11}B in polycrystalline NdB_4 at 77 K and 17.910 MHz. The upper curve is the measured one, using a measuring time of 50 min (one scan) and a peak-to-peak modulation of 6 G. The lower curves are computer simulations using the parameter values of Table I. For each site the over-all quadrupole splitting is denoted by *Q*.

deviation. Rather than emphasize this relatively unimportant deviation, we would like to stress the importance of shift anisotropies, which can be judged from the separately given simple spectra. The splittings due to anisotropy are the most important contributions to the splitting in the observed line. In fact, they dominate the differences in isotropic shifts. The second-order quadrupole splittings, indicated in Fig. 9 by Q (over-all splitting), can be seen to be relatively unimportant.

Finally, we would make some remarks on the effects of demagnetization fields. For rare-earth group-VA intermetallic compounds like CeP, Jones[5] studied the ^{31}P linewidth δH (between the extremes of the absorption derivative) in a powdered sample as a function of the volume magnetization M_V. He observed a contribution of about $3M_V$ to the linewidth and states that this is probably due to demagnetization fields. Earlier in his paper (p. 459) he remarks that the over-all shape of the sample does not influence the measured Knight shift. The demagnetization fields in the individual powder particles of various forms are thought to determine the linewidth contribution of $3M_V$. For a spherical particle, demagnetization and Lorentz fields cancel, so that one need not correct the measured Knight shifts for these fields. It is difficult to say whether or not these fields contribute slightly to the Knight shift measured in a powder of arbitrarily shaped particles. Jones considers the amount $3M_V$ as a maximum error. For NdB_4 at 77 K and 13.1 kG, $M_V = 7.2$ G, and the linewidth of the Gauss function used in the computer simulation of Fig. 9 is $2\sigma/(\gamma_{ref}/2\pi) = 15.7$ G, which is only $2.2M_V$. Moreover, this linewidth is only partially due to demagnetization effects since the Gauss-function linewidth to be used for the central line of NdB_4 at 296 K and for LaB_4 at 4.2 K appears to be $2\sigma/(\gamma_{ref}/2\pi) = 12$ G. We therefore estimate the contribution of demagnetization fields to the linewidth of NdB_4 at 77 K and 13.1 kG to be not more than $1.5M_V$. Another piece of information concerning demagnetization fields is the following. In the past we studied the Knight shift of ^{63}Cu at 300 and 77 K in the Pauli paramagnetic spinel $CuCo_2S_4$, containing 3 wt% of a second phase, CoS_2, which is ferromagnetic below 118 K. The CoS_2 ferromagnetic magnetization is not proportional to the external field H, but almost constant from 6 to 12 kG. By measuring the Knight shifts in the range of 6 to 12 kG, we could determine the extra field due to the CoS_2 magnetization. This analysis was supported by a Knight-shift determination in a sample containing only 0.4-wt% CoS_2. The over-all shape of the powder sample was a cylinder, the external field being perpendicular to its axis. The result for the sample containing 3-wt% CoS_2 was (i) a negative extra field of $-1.2M_V$ (−6 G) and (ii) a linewidth contribution of $3M_V$ (16 G). The linewidth in the sample containing 0.4-wt% CoS_2 was only 4 G at 77 K and 2.3 G at room temperature. From all this information, we estimate that $1.5M_V$ can be considered as an upper limit for the sum of the Lorentz and demagnetization fields in NdB_4 at 77 K. This amount is still 0.08% of the external field, and, if a correction is necessary, then one probably has to *add* something to the values of K_{iso} in Table I. However, it does not influence the *differences* between the isotropic shifts of the three boron sites.

V. DISCUSSION

A. Anisotropic Shifts and Principal Axes

The determination of the various parameters tabulated in Table I has been carried out under the assumption of coinciding principal axes of shift and quadrupole interaction. For sites 4*e* and 4*h* this hypothesis is valid since their point symmetries are 4 and *mm*2, respectively. We shall first discuss the shift anisotropies of 4*e* and 4*h*, and then treat the principal axes of 8*j*.

The anisotropic contributions to the observed shifts are seen to be rather large compared to the isotropic shifts K_{iso}. In order to explain this, we have calculated the dipolar fields at the boron sites due to the rare-earth magnetic moments, using our susceptibility data.[16]

For comparison with the observed quantities K'_z and ϵ (see definition in Sec. II), one has to express the dipolar shifts in terms of these parameters, i.e., as $K'_{z,dip}$ and ϵ_{dip}, but this requires a knowledge of the directions z and x in which the quadrupole interaction (absolute value) is largest and smallest, respectively. For site 4*e* this is no problem: from its axial symmetry one knows that z is along the c axis and x is anywhere in the plane perpendicular to the c axis. In Sec. IV D we already discussed that the z axis of 4*h* is also along the c axis. The axes x and y of site 4*h* make angles of 45° with the cell edges, but it remains unknown which of the two directions is the x axis. Therefore, the sign of $\epsilon_{dip}(4h)$ cannot be calculated. For the sites 4*e* and 4*h*, $K'_{z,dip}$ and $|\epsilon_{dip}|$ can now be computed. In Table II they are compared with the measured values. It can be seen that both for site

TABLE II. Observed Knight-shift anisotropies and calculated dipolar shifts for NdB_4 at 77 K.

Site	Point symmetry	K'_z (observed) (%)	$K'_{z,dip}$ (calculated) (%)	ϵ (observed)	ϵ_{dip} (calculated)
4*e*	4	−0.36(4)	−0.29	0	0
8*j*	*m*	−0.30(6)	−0.30	−0.4(2).	−0.45
4*h*	*mm*2	+0.34(4)	+0.22	$\gtrsim 0$	± 0.33

4*e* and for site 4*h* the dipolar contribution accounts for the major part of the measured shift anisotropy. This result gives firm support to the correctness of the assignment of the spectra to the sites 4*e* and 4*h*, as given in Sec. IV. A reversed assignment would imply very strong contributions (much larger than the values of the isotropic shifts) to the shift anisotropies from other than dipole origin.

We shall now discuss whether the principal axes of shift and quadrupole interaction coincide for site 8*j*. The computer program that calculates the dipolar fields also yields the principal directions of the dipolar shift tensor. At site 8*j*, one of these directions is, of course, the *c* axis, while in the plane perpendicular to it, the principal directions make angles of $\alpha = 14.6°$ with the cell edges (see Fig. 3). It is more difficult to determine the principal axes of the efg tensor. Although we realize that a point-charge model fails in explaining the *magnitude* of the observed quadrupole interactions, we think that it gives approximately the true principal *directions* of the contributions due to atoms of one site. We have tabulated values of the angle α between one of the principal directions and the cell edge, due to the atoms of different sites (Table III). Apparently, the angles α due to the different contributing neighbors do not spread very much. Moreover, the charges at 4*h* and 8*j* may be taken as equal for the following reason: The observed quadrupole interaction at site 4*h* is almost axially symmetric ($\eta < 0.05$), and on inspection of Fig. 3 one notices that the symmetry at 4*h* is not far from trigonal if the nearest neighbors (one 4*h* and two 8*j*'s) carry equal charges. This is supported by point-charge calculations. The rare-earth nearest neighbors of 4*h* constitute nearly equilateral triangles too. Returning to the problem of the principal directions of the efg at site 8*j*, we have calculated the angle α due to the equally charged atoms of 4*h* and 8*j*, the result being $\alpha = 12.2°$ (Table III). This angle is only 3.3° smaller than that due to the 4*e* atoms only, so different weighing of 4*e* and 4*h* + 8*j* will not cause much variation in the angle for the case 4*e* + 4*h* + 8*j*. Also, the angle due to the rare earths (14.6°) does not differ much from the angle of all the boron atoms (13.8°). We may therefore conclude that the angle α of the true efg at site 8*j* is about 14°. The corresponding angle of the shift tensor is probably close to that ot its dipolar contribution (14.6°). Summarizing, we think that there is good support for the assumption of nearly coinciding principal directions of shift and efg tensors at site 8*j*.

TABLE III. Angles α between principal directions of efg-tensor contributions and cell edges (*a* axes) for boron centered at site 8*j*.

Contributing neighbors with equal charges	Angle α (deg)
4*h*	6.0
8*j*	27.9
4*e*	15.5
R	14.6
4*h* + 8*j*	12.2
4*e* + 4*h* + 8*j*	13.8
4*e* + 4*h* + 8*j* + *R*	13.7

We still have to determine which of the three axes is the *x* axis and which is the *z* axis (smallest and largest quadrupole interaction, respectively) for the site 8*j*. In Fig. 8 it can be seen that the line at $H_3(8j)$ has a markedly increased intensity in the aligned sample compared to a normal sample. This line corresponds to $\theta = 90°$ and $\varphi = 0°$ (see Sec. II) or, in other words the *x* axis of site 8*j* is the direction which is turned towards the magnetic field $\vec{H}$. Therefore, the *x* axis of site 8*j* is along the *c* direction in NdB_4. There remain two possibilities for the position of the *z* axis, giving $K'_{z,\mathrm{dip}} = -0.30\%$ and $\epsilon_{\mathrm{dip}} = -0.45$, or $K'_{z,\mathrm{dip}} = +0.08\%$ and $\epsilon_{\mathrm{dip}} = +6.4$. Just as for the sites 4*e* and 4*h*, we expect the measured shift anisotropy for site 8*j* not to deviate strongly from the calculated dipolar contribution. The latter possibility is therefore to be rejected, and the first set of values for $K'_{z,\mathrm{dip}}$ and ϵ_{dip} is entered in Table II.

B. Isotropic Shifts

In Sec. I we have briefly mentioned a complication, which arises from the fact that the susceptibility is anisotropic: The dipolar fields bring about a contribution $K_{\mathrm{iso,dip}}$ to the observed shift, which cannot be distinguished from the isotropic part K_{iso}. It is proportional to the anisotropy of the susceptibility by

$$K_{\mathrm{iso,dip}} = \tfrac{1}{3} K'_{z,\mathrm{dip}} (\chi_\parallel - \chi_\perp)/\chi , \qquad (5.1)$$

where $K'_{z,\mathrm{dip}}$ stands for the dipolar part of the shift anisotropy (calculated using the isotropic part χ of the susceptibility) as tabulated in Table II. This effect is the so-called pseudocontact interaction.[3]

In order to determine the value of the correction $K_{\mathrm{iso,dip}}$, we have to know the anisotropy of the susceptibility $(\chi_\parallel - \chi_\perp)/\chi$. Since we do not have single crystals of NdB_4, we performed some measurements on aligned powder samples, yielding a lower limit for the anisotropy: $(\chi_\parallel - \chi_\perp)/\chi > 0.1$. From the fact that, in the ^{11}B NMR spectrum of the aligned sample, the $\theta = 0°$ satellites of the 4*e* and 4*h* sites have a much higher intensity than those corresponding to a random powder (Figs. 6 and 8), we conclude that the alignment of such a sample must be quite complete. Therefore, we don't expect the anisotropy of the susceptibility to be more than twice the measured value of 0.1. Taking 0.3

as a safe upper limit for the anisotropy we obtain

$$0.1<(\chi_{\parallel}-\chi_{\perp})/\chi<0.3\,. \qquad (5.2)$$

It is now a straightforward matter to find the corrections $K_{\mathrm{iso,dip}}$, using Eq. (5.1) and the calculated values of $K'_{z,\mathrm{dip}}$ (Table II). We have summarized the results in Table IV. We account for the uncertainty in the anisotropy of the susceptibility [Eq. (5.2)] by adding 0.01% to the estimated error in the corrected shifts.

In a similar way, the anisotropy of the susceptibility leads to a correction for the calculated values of $K'_{z,\mathrm{dip}}$. We shall not consider this effect, since the agreement of measured and calculated K'_z values, as presented in Table II, turned out not to change appreciably by taking this effect into account.

It is now possible to discuss the corrected isotropic shifts to the different boron sites as given in Table IV. The shifts of the three sites do not differ very much, but still we consider the difference in shift between sites $4e$ and $4h$ to be significant. We will now investigate whether we can understand this difference in terms of the Ruderman–Kittel–Kasuya–Yosida (RKKY)[1] theory as this theory has also been used to analyze the magnetic properties reported for the RB_4 compounds.[16] We write the shift as[4]

$$K=K_0[1+J(g-1)\chi_f/2gN\mu_B^2], \qquad (5.3)$$

where K_0 is the Knight shift due to the conduction-electron polarization by the external magnetic field only, g is the Landé g factor, χ_f is the molar susceptibility of the $4f$ electrons, N is Avogadro's constant, and μ_B is the Bohr magneton. In the RKKY picture, J reads as[23]

$$J=-6\pi Z\Gamma\sum_i F(2k_F R_i), \qquad (5.4)$$

where $F(x)\equiv(x\cos x-\sin x)/x^4$, Z is the number of conduction electrons per atom, Γ is the s-f exchange integral, and k_F is the conduction-electron wave vector at the Fermi surface. The summation extends over all lattice positions of magnetic ions at distances R_i from a particular boron nucleus. We have plotted these sums for the three boron sites in Fig. 10 as a function of the wave vector k_F

TABLE IV. Isotropic ^{11}B shifts in NdB_4 at 77 K, corrected for pseudocontact contributions [Eq. (5.1)], and expressed in terms of hyperfine fields per unit spin S using Eq. (5.5).

Site	K_{iso} (observed) (%)	$K'_{z,\mathrm{dip}}$ (calculated) (%)	$K_{\mathrm{iso,dip}}$ (calculated) (%)	K_{iso} (corrected) (%)	H^{hf} (kG)
$4e$	+0.33(3)	−0.29	−0.02	+0.35(4)	−2.9(3)
$8j$	+0.26(4)	−0.30	−0.02	+0.28(5)	−2.3(4)
$4h$	+0.23(3)	+0.22	+0.01	+0.22(4)	−1.8(3)

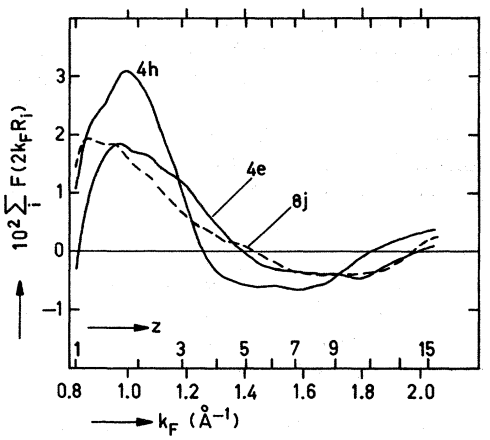

FIG. 10. Variation of the RKKY sum functions $\Sigma_i F(2k_F R_i)$ as a function of the number of conduction electrons per formula unit (z). The functions refer to the three different boron sites taken as origin.

in the region $0.8<k_F<2.0$ Å^{-1}, corresponding to $1<z<15$, z being the number of conduction electrons per unit RB_4 in the free-electron model.

In order to be able to decide whether the observed differences in isotropic shifts are in favor of the RKKY theory and incompatible with the uniform polarization model, we first have to obtain the J values [Eq. (5.3)] for the different sites. Unfortunately the necessary K_0 values (and their differences) are unknown. In the following we shall assume that they are equal and smaller than 0.03%.

We wish to stress at this point that differences in Knight shift for one kind of nucleus on different lattice sites of a nonmagnetic material are certainly not impossible. For instance, Narath[24] observed different La shifts on the two crystallographic sites of the double-hexagonal close-packed form of metallic lanthanum (the assignment of the resonances to the actual sites was impossible there because of identical quadrupole splittings).

Since the K_0's are small compared to the K_{iso}'s under discussion, and since no numerical values for the J's can be obtained, we might as well directly compare the observed shifts (to within a constant factor) with the sums in Fig. 10. Doing so, within the approximation of equal K_0's ($\ll K_{\mathrm{iso}}$'s) for the different sites, we conclude, by inspection of Fig. 10, that only at $k_F\approx1.23$ Å^{-1} and at $k_F\approx1.75$ Å^{-1} are our experimental shifts compatible with the calculated sums. If K_0 is positive, then $k_F=1.23$ Å^{-1} corresponds to $\Gamma>0$ and $k_F=1.75$ Å^{-1} corresponds to $\Gamma<0$. We remark that in our discussion of the susceptibility data[16] of the RB_4 compounds, we concluded with k_F values of around 1.7 Å^{-1}, so the data, under the given restrictions, are consistent. In view of the uncertainties regarding the K_0 values, this consistency cannot be regarded as

being experimental evidence of a nonuniform conduction-electron-spin polarization.

Finally, following Jones,[5] we shall express our results in terms of the hyperfine field H^{hf} per unit spin S, a quantity which is model independent and contains only the product $K_0 J$. It is simply related to the rate of change of the shift with the molar susceptibility:

$$H^{hf} = [gN\mu_B/(g-1)]\,\partial K/\partial\chi. \qquad (5.5)$$

The values of H^{hf} thus obtained for the different sites are tabulated in Table IV. They apparently have the usual sign and order of magnitude, as we observe from a comparison with Jones's Table VIII,[5] which gives H^{hf} values for a number of other rare-earth intermetallic compounds. In addition, we mention here that in preliminary measurements on GdB_4 and HoB_4 the shift has a different sign compared to NdB_4. However, the sign of the hyperfine fields, as defined in Eq. (5.5), is negative, showing that the direction of the spin polarization at the boron sites, relative to that of the spins $\vec{S}$ of the rare-earth ions, is the same in these compunds.

ACKNOWLEDGMENTS

The authors are indebted to R. P. van Stapele for stimulating discussions, and to P. Verburg and L. de Vries for invaluable assistance both in constructing the spectrometer and in carrying out the numerous measurements.

*Present address: Delft University of Technology, Department of Applied Physics, Lorentzweg 1, Delft, The Netherlands.

[1]M. A. Ruderman and C. Kittel, Phys. Rev. **96**, 99 (1954); T. Kasuya, Prog. Theor. Phys. **16**, 45 (1956); K. Yosida, Phys. Rev. **106**, 893 (1957).

[2]A. M. van Diepen, K. H. J. Buschow, and H. W. de Wijn, J. Chem. Phys. **51**, 5259 (1969).

[3]N. Bloembergen and W. C. Dickinson, Phys. Rev. **79**, 179 (1950); H. M. McConnell and R. E. Robertson, J. Chem. Phys. **29**, 1361 (1958).

[4]V. Jaccarino, B. T. Matthias, M. Peter, H. Suhl, and J. H. Wernick, Phys. Rev. Lett. **5**, 251 (1960); V. Jaccarino, J. Appl. Phys. Suppl. **32**, 102S (1961).

[5]E. D. Jones, Phys. Rev. **180**, 455 (1969).

[6]R. G. Barnes and B. K. Lunde, J. Phys. Soc. Jap. **28**, 408 (1970).

[7]R. B. Creel and R. G. Barnes, J. Chem. Phys. **56**, 1549 (1972).

[8]We measured $\gamma_{ref}/2\pi = 13.6601(2)$ MHz/10 kG, which agrees with the data reported by G. Lindström, Ark. Fys. **4**, 1 (1952).

[9]A. Abragam, *The Principles of Nuclear Magnetism* (Oxford U. P., London, 1961).

[10]M. H. Cohen and F. Reif, Solid State Phys. **5**, 321 (1957).

[11]This transition is usually denoted by $m \leftrightarrow m-1$. The notation $n+1/2 \leftrightarrow n-1/2$ ($n \equiv m-1/2$) makes it easier (for half-integer spins I) to see the correspondence between the mirror transitions $m \leftrightarrow m-1$ and $-(m-1) \leftrightarrow -m$. They are obtained from each other by changing the sign of n.

[12]G. H. Stauss, J. Chem. Phys. **40**, 1988 (1964).

[13]K. Narita, J. Umeda, and H. Kusumoto, J. Chem. Phys. **44**, 2719 (1966).

[14]J. F. Baugher, P. C. Taylor, T. Oja, and P. J. Bray, J. Chem. Phys. **50**, 4914 (1969).

[15]F. Wolf, D. Kline, and H. S. Story, J. Chem. Phys. **53**, 3538 (1970).

[16]K. H. J. Buschow and J. H. N. Creyghton, J. Chem. Phys. **57**, 3910 (1972).

[17]M. P. Klein and D. E. Phelps, Rev. Sci. Instrum. **38**, 1545 (1967); H. A. Buckmaster, D. J. I. Fry, and J. D. Skirrow, Rev. Sci. Instrum. **39**, 930 (1968).

[18]M. Mehring and O. Kanert, J. Sci. Instrum. **42**, 449 (1965).

[19]M. P. Klein and G. W. Barton, Rev. Sci. Instrum. **34**, 754 (1963).

[20]R. W. G. Wyckoff, *Crystal Structures*, 2nd ed. (Interscience, New York, 1964), Vol. 2.

[21]Z. Fisk, A. S. Cooper, P. H. Schmidt, and R. N. Castellano, Mater. Res. Bull. **7**, 285 (1972).

[22]A. C. Gossard and V. Jaccarino, Proc. Phys. Soc. Lond. **80**, 877 (1962).

[23]P. G. de Gennes, J. Phys. Radium **23**, 510 (1962).

[24]A. Narath, Phys. Rev. **179**, 359 (1969).